Highly Versatile Free-Standing Nano-Gold Membranes as Scaffolds for the Growth of Calcium Carbonate Crystals

Debabrata Rautaray,[†] P. Senthil Kumar,[†] Prakash P. Wadgaonkar,[‡] and Murali Sastry*,[†]

Materials Chemistry and Polymer Chemistry Divisions, National Chemical Laboratory, Pune−411 008 India

Received October 14, 2003

The growth of $CaCO_3$ crystals on free-standing carboxylic-acid-functionalized gold nanoparticle membranes is described. The gold nanoparticle membrane is synthesized by the spontaneous reduction of aqueous chloroaurate ions by a diamine molecule at a liquid−liquid interface. This membrane is robust and malleable, and most importantly, the gold nanoparticles in the membrane may be functionalized with suitable ligands. In this study, the amino acids aspartic acid and cysteine together with an aromatic bifunctional molecule, anthranilic acid, were used to modify the surface of the gold nanoparticles in the membrane. The free carboxylic acid groups on the gold nanoparticles that further functionalize these molecules were then used to bind Ca^{2+} ions, and they reacted with CO_2 to yield $CaCO_3$ crystals. The nature of the nano-gold surface modifier directed the formation of either spherical vaterite crystals or rhombohedral calcite. The nano-gold membrane thus suggests potential biomedical application as biocompatible implants, etc.

Introduction

Development of experimental processes for the synthesis of biocompatible surfaces that would induce and support mineral growth is important not only from a fundamental point of view but also in biomedical applications such as bone implants/grafting in bone surgery[1] and manufacture of artificial tissues.[2] Calcium phosphate and carbonate minerals are classified as bioactive ceramics and have been widely used for the reconstruction of bone defects.[1] In bone implant applications, inorganic composites, mainly made of hydroxyapatite [$Ca_{10}(PO_4)_6(OH)_2$] ceramics, have attracted a great deal of attention due to their excellent biocompatibility and bioaffinity.[3] However, there are critical limitations in applying the hydroxyapatites to real systems because of its poor mechanical properties, such as strength and fracture toughness. Consequently, the use of porous hydroxyapatite has been restricted to the powders, granules, and non-load-bearing small parts.[3]

Substantial progress has been made in the understanding of how biomineralization occurs and how to exploit the basic principles involved in it.[4] For instance, crystal formation during biomineralization is usually controlled in all its aspects such as orientation, size, and shape, through specialized proteins that recognize specific surfaces during the growth of the crystals. The ability of structured organic surfaces to control nucleation of crystal growth in biological and synthetic environments has prompted a number of model studies on oriented crystallization of inorganic materials using Langmuir monolayers,[5−7] self-assembled monolayers (SAMs),[8] biological macromolecules,[9] functionalized polymer surfaces,[10] and lipid bilayer stacks.[11] Attempts have also been made to control the morphology of crystals via adding suitable crystallization inhibitors[12] and carrying out crystal growth in constrained environments

* Author for correspondence. Phone: + 91 20 5893044. Fax: +91 20 5893952/5893044. E-mail: sastry@ems.ncl.res.in.

[†] Materials Chemistry Division.

[‡] Polymer Chemistry Division.

(1) Schnettler, R.; Alt, V.; Dingeldein, E.; Pfefferle, H. J.; Kilian, O.; Meyer, C.; Heiss, C.; Wenisch, S. *Biomaterials* **2003**, *24*, 4603.

(2) Dolder, J. V. D.; Farber, E.; Spauwen. P. H. M.; Jansen, J. A. *Biomaterials* **2003**, *24*, 1745.

(3) Kim, H. W.; Lee, S. Y.; Bae, C. J.; Noh, Y. J.; Kim, H. E.; Kim, H. M.; Ko, J. S. *Biomaterials* **2003**, *24*, 3277.

(4) Heuer, A. H.; Fink, D. J.; Laraia, V. J.; Arias, J. L.; Calvert, P. D.; Kendall, K.; Messing, G. L.; Blackwell, J.; Rieke, P. C.; Thomoson, D. H.; Wheeler, A. P.; Veis, A.; Caplan, A. I. *Science* **1992**, *255*, 1098.

(5) Litvin, A. L.; Valiyaveettil, S.; Kaplan, D. L.; Mann, S. *Adv. Mater.* **1997**, *9*, 124.

(6) Heywood, B. R.; Mann, S. *Adv. Mater.* **1994**, *6*, 9 and references therein.

(7) Buijnsters, P. J. J. A.; Donners, J. J. J. M.; Hill, S. J.; Heywood, B. R.; Nolte, R. J. M.; Zwanenburg, B.; Sommerdijk, N. A. J. M. *Langmuir* **2001**, *17*, 3623.

(8) (a) Kuther, J.; Nelles, G.; Seshadri, R.; Schaub, M.; Butt, H.-J.; Tremel, W. *Chem. Eur. J.* **1998**, *4*, 1834. $CaCO_3$: (b) Aizenberg, J.; Black, A. J.; Whitesides, G. M. *J. Am. Chem. Soc.* **1999**, *121*, 4500. (c) Travaille, A. M.; Donners, J. J. J. M.; Gerritsen, J. W.; Sommerdijk, N. A. J. M.; Nolte, R. J. M.; Kempen, H. V. *Adv. Mater.* **2002**, *14*, 492−495.

(9) Falini, G.; Albeck, S.; Weiner, S.; Addadi, L. *Science* **1996**, *271*, 67.

(10) (a) Feng, S.; Bein, T. *Science* **1994**, *265*, 1839. (b) Falini, G.; Gazzano, M.; Ripamonti, A. *Adv. Mater.* **1994**, *6*, 46. (c) Donners, J. J. J. M.; Nolte, R. J. M.; Sommerdijk, N. A. J. *J. Am. Chem. Soc.* **2002**, *124*, 9700−9701.

(11) (a) Damle, C.; Kumar, A.; Bhagwat, M.; Sainkar, S. R.; Sastry, M. *Langmuir* **2002**, *18*, 6075. (b) Rautaray, D.; Kumar, A.; Reddy, S.; Sainkar, S. R.; Sastry, M. *Cryst. Growth Des.* **2002**, *2*, 197. (c) Sastry, M.; Kumar, A.; Damle, C.; Sainkar, S. R.; Bhagwat, M.; Ramaswami, V. *CrystEngComm* **2001**, 21. (d) Rautaray, D.; Sainkar, S. R.; Sastry, M. *Langmuir* **2003**, *19*, 888. (e) Rautaray, D.; Sainkar, S. R.; Sastry, M. *Chem. Mater.* **2003**, *15*, 2809.

(12) (a) Bromley, L. A.; Cottier, D.; Davey, R. J.; Dobbs, B.; Smith, S.; Heywood, B. R. *Langmuir* **1993**, *9*, 3594. (b) Qi, L.; Coffen, H.; Antonietti, M. *Angew. Chem., Int. Ed.* **2000**, *39*, 604. (c) Uchida, M.; Sue, A.; Yoshioka, T.; Okuwaki, A. *CrystEngComm* **2001**, 5.

10.1021/cm035004s CCC: $27.50
Published on Web 02/18/2004

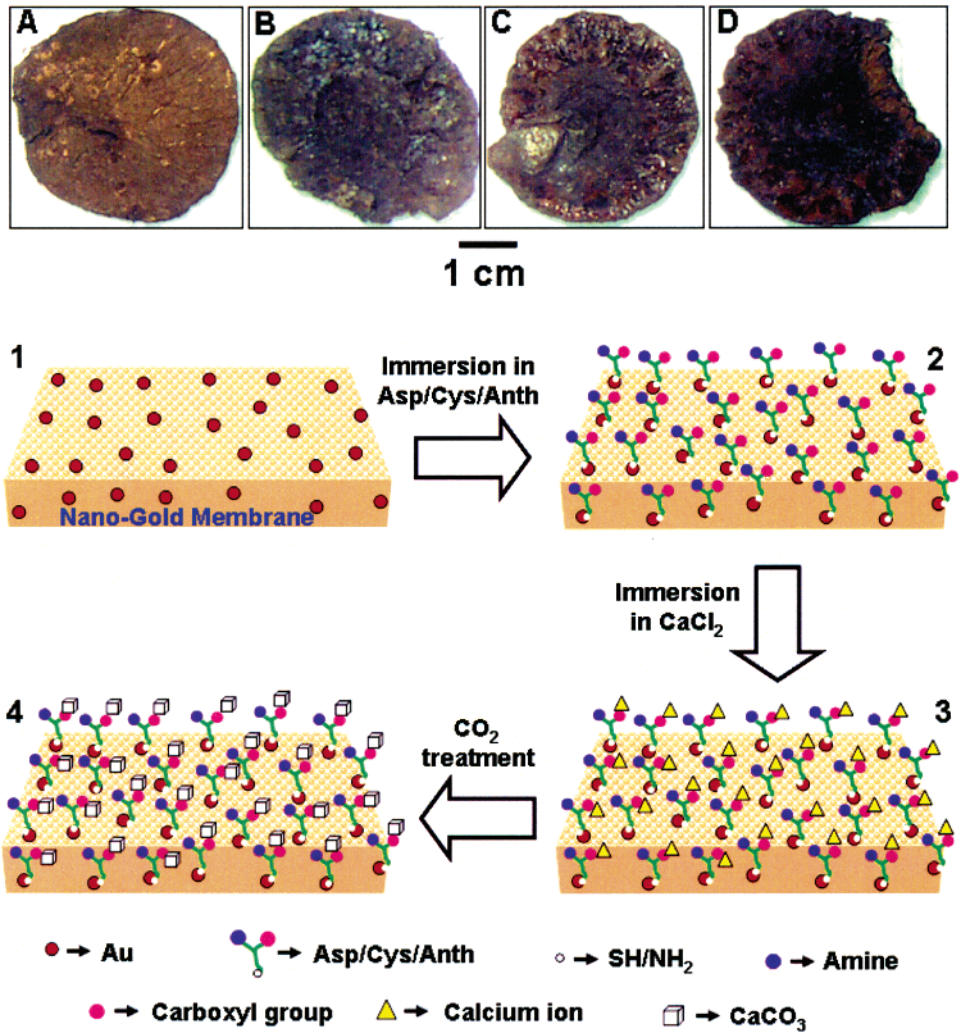

Figure 1. (A) Photograph of the air-dried, as prepared, free-standing gold nanoparticle membrane. (B−D) Photographs of $CaCO_3$ crystals grown on aspartic-acid-, cysteine-, and anthranilic-acid-functionalized gold nanoparticle membranes, respectively (scale bar is same for all). Scheme showing different steps involved during the growth of $CaCO_3$ crystals on free-standing gold nanoparticle membrane. Step 1 shows as prepared gold nanoparticle membrane. Step 2 shows functionalization of the gold nanoparticle membrane by aspartic acid, cysteine, and anthranilic acid, respectively. Step 3 shows immobilization of Ca^{2+} ions to the functionalized gold nanoparticle membrane. Step 4 shows Ca^{2+}−nano-gold membrane after reaction with CO_2.

such as those afforded by microemulsions[13] or at the interface between two liquids.[14]

It is clear from the above that while a plethora of biocompatible surfaces do exist for mineral growth, very few of them actually present malleable/ductile materials that could be suitably molded for bone-implant applications. With this goal in mind, we have investigated the possibility of using membranes of gold nanoparticles in a polymeric background for mineral growth. There are two main reasons for using a gold nanoparticle membrane in such an application. The first is that polymeric membranes would be simple to handle and sculpt to the desired shape and size. The second is that the chemistry pertaining to surface modification of gold nanoparticles is very well understood. Indeed, gold nanoparticles have been routinely bioconjugated with amino acids,[15] proteins,[16] and DNA.[17] It should therefore be relatively straightforward to derivatize the gold nanoparticle membrane with functional groups capable of inducing mineral growth.

In the remainder of this article, we demonstrate that a free-standing gold nanoparticle membrane synthesized at the interface between chloroform containing bis-(2-(4-aminophenoxy)ethyl)ether (DAEE) and aqueous chloroauric acid solution (photograph A in of Figure 1) and thereafter functionalized with the amino acids, cysteine and aspartic acid, as well as the bifunctional

(13) (a) Hopwood, J. D.; Mann, S. *Chem. Mater.* **1997**, *9*, 950. (b) Li, M.; Mann, S. *Langmuir* **2000**, *16*, 7088. (c) Hopwood, J. D.; Mann, S. *Chem. Mater.* **1997**, *9*, 1819. (d) Summers, M.; Eastoe, J.; Davis, S. *Langmuir* **2002**, *18*, 5023−5026.

(14) (a) Rautaray, D.; Kumar, A.; Reddy, S.; Sainkar, S. R.; Pavaskar, N. R.; Sastry, M. *CrystEngComm* **2001**, *45*, 1. (b) Reddy, S.; Rautaray, D.; Sainkar, S. R.; Sastry, M. *Bull. Mater. Sci.* **2003**, *26*, 283.

(15) (a) Selvakannan, P. R.; Mandal, S.; Phadtare, S.; Gole, A.; Pasricha, R.; Adyanthaya, S.; Sastry, M. *J. Colloids Interface Sci.* **2004**, *269*, 97. (b) Selvakannan, P. R.; Mandal, S.; Phadtare, S.; Pasricha, R.; Sastry, M. *Langmuir* **2003**, *19*, 3545. (c) Mandal, S.; Selvakannan, P. R.; Phadtare, S.; Pasricha, R.; Sastry, M. *Proc. Indian Acad. Sci., Chem. Sci.* **2002**, *114*, 513.

(16) (a) Gole, A.; Dash, C.; Ramakrishnan, V.; Sainkar, S. R.; Mandale, A. B.; Rao, M.; Sastry, M. *Langmuir* **2001**, *17*, 1674. (b) Gole, A.; Dash, C.; Soman, C.; Sainkar, S. R.; Rao, M.; Sastry, M. *Bioconjugate Chem.* **2001**, *12*, 684. (c) Gole, A.; Vyas, S.; Phadtare, S.; Lachke, A.; Sastry, M. *Colloids Surf., B* **2002**, *25*, 129. (d) Zhao, J.; O'Daly, J. P.; Henkens, R. W.; Stonehuerner, J.; Crumblis, A. L. *Biosens. Bioelectron.* **1996**, *11*, 493. (e) Keating, C. D.; Kovaleski, K. M.; Natan, M. J. *J. Phys. Chem. B* **1998**, *102*, 9404.

(17) Park, S.; Taton, T. A.; Mirkin, C. A. *Science* **2001**, *295*, 1503.

molecule, anthranilic acid ($H_2N-C_6H_4-COOH$), is an excellent material for the growth of $CaCO_3$. The membrane is formed spontaneously by the reduction of $AuCl_4^-$ ions by DAEE, this process leading to the formation of gold nanoparticles. The concomitant process of oxidation of DAEE leads to the creation of a polymeric matrix in which the gold nanoparticles are embedded. The gold nanoparticle membrane is extremely stable, robust, easily handled (see photograph A at the top of Figure 1), and malleable, and it can be grown over large areas and thicknesses by suitably varying the experimental conditions.[18] We have chosen $CaCO_3$ as a model system to test the mineral growth capability of our gold nanoparticle membrane since it is a relatively complex mineral system due to the existence of the three polymorphs calcite, aragonite, and vaterite. It is also the most widely studied biomineral. $CaCO_3$ growth on suitably functionalized gold nanoparticle membranes was accomplished by first electrostatically complexing Ca^{2+} ions with gold nanoparticle surface-bound carboxylic acid groups (by immersion of the membrane in aqueous $CaCl_2$ solution) and, thereafter, exposing this material to CO_2 gas. Facile growth of $CaCO_3$ crystals was observed within 1 h of gassing. Interestingly, we observe the presence of the unstable polymorph vaterite along with calcite in the three membranes studied, the relative percentage of the two polymorphs being dependent on the nature of surface modifier. Presented below are details of the investigation.

Experimental Details

Chemicals Used. Chloroauric acid, bis(2-(4-aminophenoxy)-ethyl)ether (DAEE), aspartic acid, cysteine, anthranilic acid, calcium chloride, and ammonium carbonate were obtained from Aldrich Chemicals and used as received.

Nano-Gold Membrane Preparation. In a typical experiment, 30 mL of 10^{-3} M chloroauric acid ($HAuCl_4$) and 30 mL of 10^{-3} M bis(2-(4-aminophenoxy)ethyl)ether (DAEE) in $CHCl_3$ were mixed in a beaker kept under static ambient conditions in the dark for 3 h. After 3 h of reaction, a purple membrane was observed to have formed at the organic/aqueous liquid−liquid interface. After the removal of the aqueous component of the biphasic mixture, the nano-gold membrane was lifted with forceps, washed thoroughly several times with double distilled water, and dried before further use (photograph A, Figure 1, and scheme in Figure 1, step 1).

Functionalization of the Nano-Gold Membrane. The surface modification of the nano-gold membranes was done by immersing the as-prepared nano-gold membranes in 50 mL of aqueous solutions of 10^{-4} M aspartic acid and cysteine as well as the bifunctional molecule anthranilic acid ($H_2N-C_6H_4-COOH$) separately for 30 min, respectively. After surface functionalization, the nano-gold membranes were washed thoroughly several times with double distilled water and dried before further use (scheme in Figure 1, step 2).

Calcium Carbonate Crystal Growth. The growth of $CaCO_3$ crystals was achieved by simple immersion of the functionalized (aspartic acid, cysteine and anthranilic acid) nano-gold membranes in 50 mL of 10^{-3} M aqueous $CaCl_2$ solution for 3 h. The resulting Ca^{2+}-functionalized gold membranes were washed several times thoroughly with double distilled water and dried under flowing nitrogen (scheme in Figure 1, step 3). Thereafter, the growth of calcium carbonate crystals was achieved by exposing the different nano-gold membranes to CO_2 atmosphere [produced by decomposition of $(NH_4)_2CO_3$)] for 1 h (scheme in Figure 1, step 4). Consequent to formation of $CaCO_3$ crystals, the color of the membrane changed from purple to a dull/dark gray (photographs B−D, Figure 1). The resultant $CaCO_3$−nano-gold membranes were washed with double distilled water several times prior to analysis.

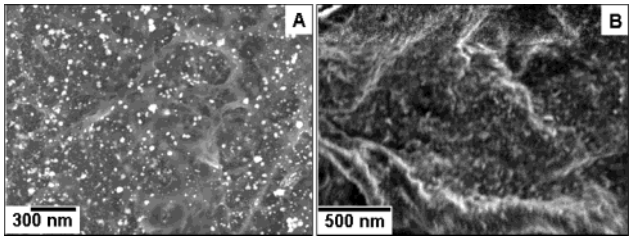

Figure 2. (A) SEM micrograph of the as-prepared, free-standing gold nanoparticle membrane. (B) SEM micrograph of the $CaCO_3$ crystals grown on the as-prepared gold nanoparticle membrane without any surface modification.

The $CaCO_3$−nano-gold membranes at different stages of synthesis were characterized using a variety of techniques. Fourier transform infrared spectroscopy (FTIR) measurements were carried out in the diffuse reflectance mode (keeping the nonfunctionalized nano-gold membrane as the standard) at a resolution of 4 cm^{-1} on a Perkin-Elmer FTIR−Spectrum One instrument. X-ray diffraction (XRD) measurements of the membranes were carried out in the transmission mode on a Philips PW 1830 instrument operating at 40 kV voltage and a current of 30 mA with Cu Kα radiation. Scanning electron microscopy (SEM) measurements of the nano-gold membranes were carried out on a Leica Stereoscan-440 instrument equipped with a Phoenix energy dispersive analysis of X-rays (EDAX) attachment.

Results and Discussion

As briefly mentioned above, the purple gold nanoparticle membrane that formed at the interface between chloroform and water was free-standing and could easily be handled using forceps indicating its robust character (photograph A in Figure 1). Figure 2A shows a representative SEM image of the as-prepared gold nanoparticle membrane. The as-prepared membrane shows a very uniform polymeric background in which gold nanoparticles are embedded, and it is hydrophilic in nature (a contact angle of 45° is observed). The gold nanoparticles themselves appear as bright and almost spherical structures. Selected area energy dispersive analysis of X-rays (EDAX) measurements carried out on the spherical structures (curve 1 in Supporting Information, Figure S1) indicated that they were indeed gold particles. Along with a prominent Au peak, N, C, and O signals were also observed in the EDAX spectrum representative of the polymeric network (curve 1 in Figure S1) and are consistent with the chemical composition of the DAEE precursor. The size of the gold nanoparticles in the membrane was estimated to be in the range 80−350 nm. The weight percentage contribution of the gold component in the membrane was estimated by thermogravimetric analysis (data not shown) to be ca. 35%. Curve 1 in Figure 3 shows the XRD pattern recorded from the gold nanoparticle membrane. The Bragg reflections in the as-prepared gold nanoparticle membrane clearly correspond to the fcc crystalline structure of gold.[19]

(18) Selvakannan, PR.; Kumar, P. S.; More, A. S.; Shingte, R. D.; Wadgaonkar, P. P.; Sastry, M. Manuscript in preparation.

(19) Selvakannan, P. R.; Mandal, S.; Pasricha, R.; Adyanthaya, S. D.; Sastry, M. *Chem. Commun.* **2002**, 1334.

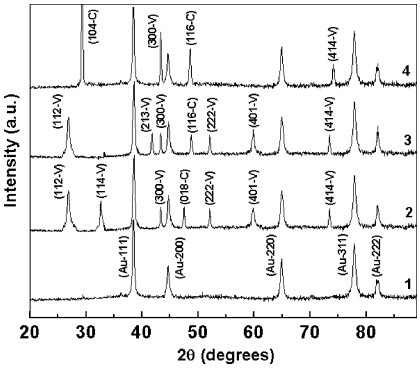

Figure 3. XRD patterns recorded from the as-prepared gold nanoparticle membrane (curve 1), and $CaCO_3$ crystals grown on aspartic-acid-functionalized (curve 2), cysteine-functionalized (curve 3), and anthranilic-acid-functionalized (curve 4) gold nanoparticle membrane. The Bragg reflections have been indexed (C stands for calcite and V stands for vaterite, see text for details).

Figure 1B−D shows photographs of $CaCO_3$ crystals grown on aspartic acid, cysteine, and anthranilic acid functionalized gold nanoparticle membranes, respectively. Upon formation of $CaCO_3$ crystals on the functionalized gold nanoparticle membranes, lots of white bright spots can clearly be seen (Figure 1B−D) attributed to $CaCO_3$ crystal growth, in contrast to the as-prepared nano-gold membrane (purple in color, Figure 1A). The scheme in Figure 1 shows the different steps involved during the growth of $CaCO_3$ crystals by using a free-standing gold nanoparticle membrane as a scaffold. The first step in our study is the preparation of a nano-gold membrane (step 1) followed by the functionalization of the nano-gold membrane by carboxyl terminated aspartic acid, cysteine, and anthranilic acid, respectively (step 2), which then were separately subjected to Ca^{2+} ion immobilization (step 3). Thereafter, the reaction of Ca^{2+}−nano-gold membrane with CO_2 resulted in the formation of $CaCO_3$ crystals (step 4).

The nano-gold membrane was then derivatized by immersion in aqueous solutions of the amino acids cysteine and aspartic acid as well as the bifunctional molecule, anthranilic acid. The choice of these surface modifiers and their possible influence on the crystallography and morphology of the $CaCO_3$ crystals grown on the membranes was motivated by the following reasons. In the case of aspartic acid and anthranilic acid, binding with the gold nanoparticles is expected to occur through the amine functional groups[20] leaving the carboxylic acid groups free to complex with Ca^{2+} ions. Anthranilic acid was chosen to see if the presence of an aromatic group in the molecule would affect the crystallography and morphology of $CaCO_3$ crystals grown on the membrane scaffold. In the case of cysteine modification of the nano-gold membrane, thiol groups would compete with the amine group for binding with the gold nanoparticles,[21] thus leading to a nano-gold membrane with a surface less acidic than that of the aspartic acid modified membrane.

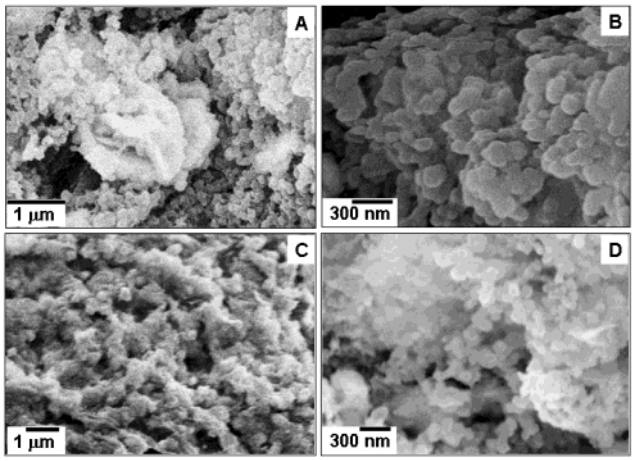

Figure 4. (A,B) SEM micrographs at different magnifications of $CaCO_3$ crystals grown on aspartic-acid-functionalized gold nanoparticle membrane. (C,D) Micrographs at different magnifications of $CaCO_3$ crystals grown on cysteine-functionalized gold nanoparticle membrane (see text for details).

Figure 4A,B shows representative SEM images of $CaCO_3$ crystals grown on the aspartic-acid-functionalized gold nanoparticle membrane. At low magnification, it is seen that the membrane is very uniformly and densely covered with $CaCO_3$ (Figure 4A). At higher magnification (Figure 4B), the $CaCO_3$ component is clearly seen to be made up of aggregates of quasispherical $CaCO_3$ crystals. Spot profile EDAX analysis of the Ca^{2+}−nano-gold membrane and after formation of $CaCO_3$ crystals shown in Figure 4A,B is shown in curves 2 and 3 in Figure S1, respectively. Along with Au, C, N, and O, a strong Ca signal can be seen in the Ca^{2+}−nano-gold membrane (curve 2, Figure S1). The EDAX spectrum after the formation of $CaCO_3$ membrane clearly shows an increase in the C and O signals upon reaction with CO_2 indicating the formation of $CaCO_3$ crystals. An analysis of the EDAX data yielded an average Ca/C/O atomic ratio of 1:2.3:3.6. The excess C and O in the elemental ratio is attributed to the contribution from the underlying polymer membrane (curve 3, Figure S1). Strong Au and N signals were also observed from the membrane and arise due to the nanoparticles and aspartic acid, respectively. The XRD pattern recorded from the $CaCO_3$ crystals grown on the aspartic acid derivatized nano-gold membrane is shown as curve 2 in Figure 3. A number of Bragg reflections are identified and agree excellently with those reported for vaterite (peaks designated with a V).[22] A very small calcite contribution is also observed (peaks designated with a C). The XRD data thus provide clear support for the morphology of the $CaCO_3$ crystals seen in the SEM images; such well-defined spherical structures are known to be characteristic of the vaterite polymorph.[9] Further evidence of vaterite formation is provided by FTIR analysis of the $CaCO_3$−aspartic-acid−nano-gold membrane (curve 2, Figure 5). The absorption bands centered at 877 and 746 cm^{-1} are characteristic of vaterite.[9] Along with the absorption bands for vaterite, a very weak absorption band can be seen at 712 cm^{-1} in this membrane and is attributed to the small

(20) Kumar, A.; Mandal, S.; Selvakannan, P. R.; Pasricha, R.; Mandale, A. B.; Sastry, M. *Langmuir* **2003**, *19*, 6277.

(21) (a) Brust, M.; Walker, M.; Bethell, D.; Schiffrin, D. J.; Whymann, R. *Chem. Commun.* **1994**, 801. (b) Mayya, K. S.; Patil, V.; Sastry, M. *Langmuir* **1997**, *13*, 3944.

(22) Nassrallah-Aboukais, N.; Boughriet, A.; Laureyns, J.; Aboukais, A.; Fischer, J. C.; Langelin, H. R.; Wartel, M. *Chem. Mater.* **1998**, *10*, 238.

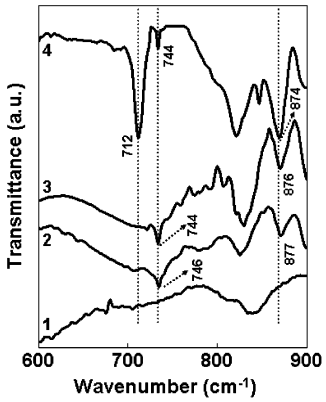

Figure 5. FTIR spectra recorded from the as-prepared gold nanoparticle membrane (curve 1), and the aspartic-acid-functionalized (curve 2), cysteine-functionalized (curve 3), and anthranilic-acid-functionalized (curve 4) gold nanoparticle membranes after formation of $CaCO_3$.

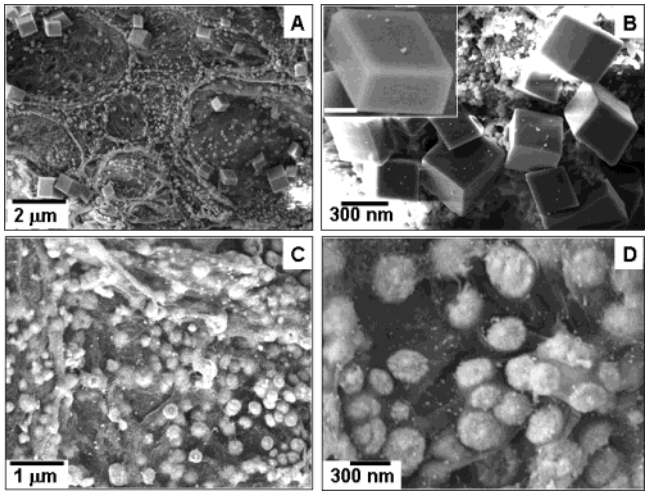

Figure 6. (A−D) Representative SEM micrographs recorded at different magnifications of $CaCO_3$ crystals grown on anthranilic-acid-functionalized gold particle membrane (see text for details). The inset in part B shows a higher magnification SEM micrograph of one of the rhombohedral $CaCO_3$ crystals in greater detail (scale bar is 100 nm).

percentage of calcite present in the sample. The vaterite−aspartic-acid−nano-gold membrane was then immersed in alkali solution to dissolve the $CaCO_3$ component. From the difference in weight of the membrane before and after $CaCO_3$ removal, the weight percentage contribution of $CaCO_3$ to the nano-gold membrane was estimated to be 2.11%.

Figure 4C,D shows SEM images of $CaCO_3$ crystals grown on the cysteine-functionalized gold nanoparticle membrane. As in the case of the aspartic-acid-modified nano-gold membrane, the low magnification SEM image (Figure 4C) shows extremely dense coverage of $CaCO_3$ crystals over the membrane surface and within pores of the membrane. At higher magnification (Figure 4D), the crystals are seen clearly to be composed of spherical $CaCO_3$ crystals similar to those observed in the aspartic-acid-modified nano-gold membrane (Figure 4A,B) with the only difference being that the crystals are smaller and apparently more uniform in size in the case of the aspartic-acid-modified nano-gold membrane. EDAX analysis of the $CaCO_3$ crystals yielded a Ca/C/O atomic ratio of 1:2.7:3.35 (curve 4 in Figure S1), and as earlier, the excess C and O signals likely arise from the polymer membrane. Strong Au and N signals were also observed from the membrane and arise due to the nanoparticles and cysteine, respectively. The XRD pattern recorded from the $CaCO_3$ crystals shown in Figure 4C,D is shown as curve 3 in Figure 3. A number of Bragg reflections are identified and agree with those reported for vaterite.[22] There is also evidence for a small percentage of calcite in the aspartic-acid-modified membrane. Further evidence of vaterite formation is provided by FTIR analysis (curve 3 in Figure 5). The absorption bands centered at 877 and 744 cm^{-1} are characteristic of vaterite[9] and are observed along with a small absorption band at 712 cm^{-1} which is attributed to the presence of a small percentage of calcite in the sample. The contribution of $CaCO_3$ to the nano-gold membrane was estimated to be ca. 2.19 wt %. Vaterite is thermodynamically the most unstable polymorph of the three crystal structures of $CaCO_3$ and is used for specific applications requiring high specific surface area, high solubility, high dispersion, and smaller specific gravity. We speculate that the vaterite surface was stabilized by the carboxylic acid-terminated aspartic acid and cysteine molecules that also prevent their phase transformation to calcite.

The crystallization of $CaCO_3$ was also studied using the bifunctional molecule anthranilic acid as a surface modifier for the nano-gold membrane. This molecule binds to nano-gold through the amine functionality thus exposing carboxylic acid groups on the surface of the nanoparticles. Anthranilic acid possesses an aromatic group, and it would be interesting to study the effect of this group. Figure 6A−D shows representative SEM images of the $CaCO_3$ crystals grown on anthranilic-acid-functionalized gold nanoparticle membrane. The low magnification SEM image (Figure 6A) shows $CaCO_3$ crystals densely populating the nano-gold membrane surface. The $CaCO_3$ crystals are composed of spherical and rhombohedral structures. At higher magnification (Figure 6B), highly faceted rhombohedral $CaCO_3$ crystals are observed. The inset in Figure 6B clearly shows one of the faceted rhombohedral $CaCO_3$ crystals in greater detail. Figure 6C,D shows low and high magnification SEM images of spherical $CaCO_3$ crystals present along with the rhombohedral shaped $CaCO_3$ crystals grown on the anthranilic-acid-functionalized nano-gold membrane shown in Figure 6A. The low magnification SEM image (Figure 6C) clearly shows spherical $CaCO_3$ crystals populating the membrane surface along with rhombohedral crystals. The higher magnification SEM image (Figure 6D) clearly reveals that the individual spherical structures are in turn composed of very small individual crystallites of $CaCO_3$ by an aggregation process. EDAX analysis of the $CaCO_3$ crystals yielded a Ca/C/O atomic ratio of 1:2.8:3.7 along with the expected Au and N signals from the membrane as well (curve 5 in Figure S1). The XRD pattern recorded from the $CaCO_3$ crystals shown in Figure 6 is shown as curve 4 in Figure 3. A number of Bragg reflections are identified and have been indexed with reference to the unit cell of the calcite[8a,22] and vaterite structure.[22] The XRD results suggest some oriented growth of the rhomobohedral calcite crystals along the (104) direction. The SEM and XRD results clearly show

that, in the case of anthranilic-acid-functionalized nano-gold membrane, $CaCO_3$ crystals of mixed polymorphs (calcite and vaterite) were nucleated and grown on the membrane. Further evidence of the formation of both calcite and vaterite crystals in this experiment is provided by FTIR analysis of the membrane (curve 4 in Figure 5). The absorption bands centered at 874 and 712 cm^{-1} are characteristic of calcite[9] whereas the 744 cm^{-1} absorption band is characteristic of vaterite.[9] The weight percentage contribution of the $CaCO_3$ component in the anthranilic-acid-functionalized nano-gold membrane was estimated to be 2.32%.

To understand better the role played by the surface functionality of the nano-gold membrane in stabilizing the unstable vaterite phase and growth of oriented calcite crystals, a control experiment was performed wherein $CaCO_3$ crystallization was achieved using the as-prepared nano-gold membrane (without any surface functionalization) as a crystallizing template. Figure 2B shows the SEM picture of the nano-gold membrane in this control experiment after $CaCO_3$ growth. While some reorganization of the membrane can be seen (compare with Figure 2A), there is no evidence for the presence of $CaCO_3$ crystals on the surface of the membrane. EDAX and XRD analysis of the membrane (data not shown) support this claim. It is thus evident that modification of the membrane with functional groups capable of binding Ca^{2+} ions is an essential prerequisite for the formation of $CaCO_3$ crystals on the membrane.

The need of surface modification and the chemical binding process of the nano-gold membrane is discussed below. We have chosen aspartic acid and cysteine to modify the surface of the gold nanoparticle membrane for the following reasons: (a) the use of an amino acid would more closely approximate a biological surface; (b) aspartic acid and cystenine contain amine/thiol groups that are known to bind strongly with gold nanoparticles,[15c] and therefore, free carboxylic acid groups in the amino acid would be present at the surface of the nano-gold membrane during immersion in $CaCl_2$ solution (pH 6.5).

It is clear that the nature of surface modification through the carboxylic acid functional groups determines the nature of $CaCO_3$ crystals grown on the surface of the nano-gold membrane. At this stage it is not clear whether the surface topography (dictated by the gold nanoparticles embedded in the polymer membrane) also contributes to the spherical vaterite crystals grown on the membrane surface. However, the fact that anthranilic-acid-modified nano-gold membrane initiated growth of calcite crystals over vaterite indicates that the surface modifier plays a more crucial role. We are currently working on understanding how the different crystal morphologies and indeed crystallography are directed by the nano-gold membrane surface modified in terms of registry between the carboxylic acid surface and various crystal planes of calcite/vaterite.

In conclusion, this paper describes the oriented growth of calcite and stabilization of the unstable polymorph vaterite on the surface of carboxylic-acid-functionalized gold nanoparticle membrane. The nano-gold membrane was formed spontaneously by the reaction of bis(2-(4-aminophenoxy)ethyl)ether with aqueous chloroaurate ions at the liquid−liquid interface and, thereafter, surface-modified with the amino acids aspartic acid and cysteine as well as the bifunctional molecule anthranilic acid. $CaCO_3$ growth was achieved by binding Ca^{2+} ions to the nano-gold surface-bound carboxylic acid followed by reaction with CO_2. The nature of $CaCO_3$ crystals formed was found to be a strong function of the nano-gold surface modifier. The ability to grow free-standing, robust, and malleable nano-gold membranes that may be derivatized to induce and support inorganic crystal growth has important implications in biomedical applications such as bone implants.

Acknowledgment. D.R. thanks the Department of Science and Technology (DST), Government of India, for financial assistance. P.S.K. thanks the Council of Scientific and Industrial Research (CSIR), Government of India, for a research associateship. This work was partially funded by grants to M.S. from the DST and the Indo-French Centre for the Promotion of Advanced Scientific Research (IFCPAR, New Delhi), and these organizations are gratefully acknowledged.

Supporting Information Available: EDAX spectra recorded from the nano-gold membrane at different stages of surface modification and $CaCO_3$ growth (Figure S1). This material is available free of charge via the Internet at http://pubs.acs.org.

CM035004S